Semiconductor Detectors

J.R. Powers-Luhn

NE550, Thursday 17:30

April 27, 2017

1 Abstract

The performance of two different types of semiconductor detectors, High Purity Germanium (HPGE) and Cadmium Zinc Telluride (CZT), were examined and compared for a variety of pure, sealed sources. Calculations were made for the resolution of known peaks (using a gaussian curve fitting technique), linearity of response to radiation (via a linear least-squares fit to well characterized sources), and photopeak response for each detector material. In addition, an attempt was made to examine the geometric efficiency of the HPGe detector as a function of distance from a near point source, with qualitative evaluation of the impact of deadtime. Spectra for an assortment of sources and detectors are provided with notable features identified on their plots.

2 Introduction

Semiconductor detectors are useful for collecting detailed spectra for radiation sources. Their higher density (HPGe has a density of $5.32\,\mathrm{g/cm^2}$ [1]) allows much smaller detectors than gas detectors, with the additional advantage of shorter deadtimes. Additionally, they exhibit dead times significantly lower than gas detectors, often by several orders of magnitude [2]. Furthermore, in contrast to scintillation detectors, they do not require the use of coupled photomultiplier tubes with the efficiency losses implied.

Semiconductor detectors have electrons that occupy outer shells below the conduction band when they are at rest. When they are biased with an appropriate voltage, the gap between the valence band and the conduction band shrinks to a value that can be bridged by the introduction of ionizing radiation. These band gaps tend to be low–1.572 eV for CZT at 300K [3]. This can introduce additional problems in very sensitive materials such as HPGe, where thermal excitations can cause increased noise due to spontaneous conduction (without an inciting ionizing event). As a result, HPGe detectors must be cooled by liquid nitrogen or by complicated mechanical cooling means.

While the semiconductor detectors are generally very performant, they are not identical. The size of the band gap, and therefore the resolution that they can provide, varies from material to material. Additionally, different materials exhibit different cross sections for various ranges of radiation, meaning that they have different responses to ionizing events. These changes introduce various tradeoffs that must be made between detector materials, including convenience and price in addition to efficiency and resolution.

In order to characterize the latter two tradeoffs, measurements were made for an assortment of sealed sources with known spectra using two types of detectors: high purity Germanium and Cadmium Zinc Telluride. These spectra were taken with a standardized chain of nuclear instrumentation and Maestro MCA software. A moderately-well characterized background was taken in order to directly compare the response of the detectors.

3   Experimental

3.1   MCA Linearity

In order to determine the linearity response of the ORTEC 927 ASPEC MCA, a model BNC BL-2 voltage pulse generator was connected through an ORTEC 572A amplifier to the MCA while the output of the pulse generator was also monitored via an GW INSTEK model GDS-3254 oscilloscope, as indicated in figure 1. The output of the MCA was recorded in the Maestro software for several voltage settings, and the channels corresponding to each peak recorded.
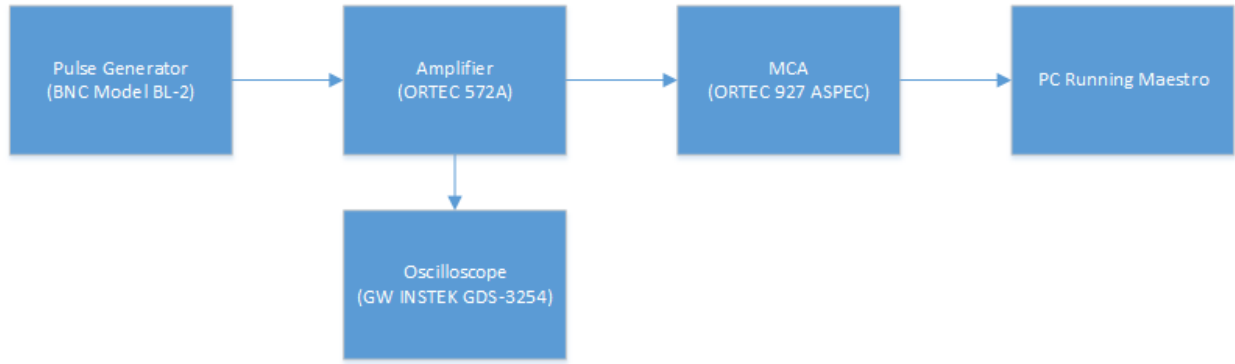
Figure 1: MCA experiment block diagram

3.2 MCA Dead Time

In order to determine the dead time of the MCA, the pulse generator was then set to produce a double pulse with a 3 µs rise time and a 10 µs fall time. Amplifier shaping time was set to 0.5 µs with an amplitude of 5.44 V. The MCA was set to conduct a continuous collection with a 12 bit conversion gain. The spacing between the pulse was adjusted and the threshold at which the MCA was able to distinguish between the pulses (the point at which two peaks appeared on the spectrum) recorded.

3.3 HPGe Evaluation

The MCA was then connected to an HPGe/Preamplifier/Amplifier chain as indicated in figure 2. The amplifier shaping time was set to 10 µs with a gain setting of 10 and unipolar output. After a 10 min background was collected, an assortment of sealed sources were placed at a distance of approximately 10 cm from the detector face. Information regarding the sources is presented in table 1. Spectra for these sources were collected in the highest-available number of channels (14 bits) in order to take advantage of the high resolution of the HPGe detector. Sources were counted for 150 s in order to obtain sufficient counts to obtain reasonable statistics.
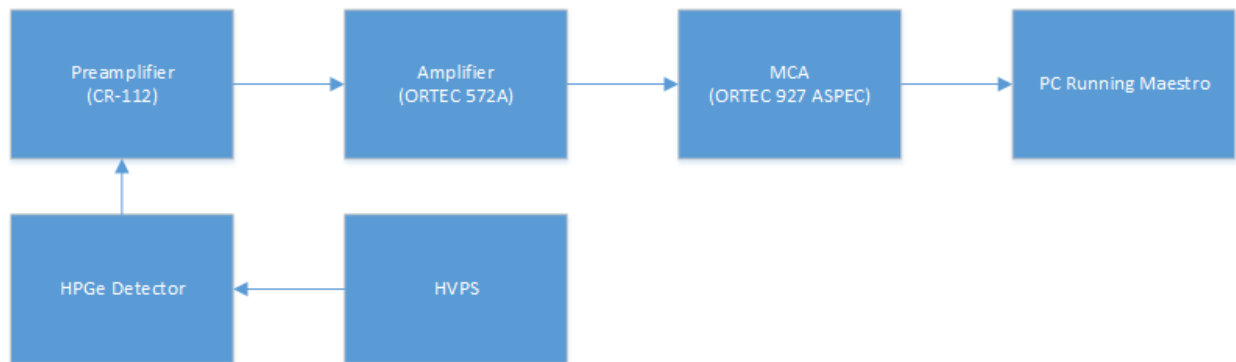
3

Figure 2: HPGe experiment block diagram

Table 1: Sources for HPGe Evaluation

Source	Date	Activity
Na-22	April 2015	1 μCi
Cs-137	April 2015	10 μCi
Co-60	May 2012	1 μCi
Mn-54	February 2012	10 μCi
Cd-109	May 2015	1 μCi
Ba-133	February 2012	1 μCi
Co-57	May 2015	1 μCi

Table 2: Sources and count time for CZT evaluation

Source	Count time (s)
Na-22	300
Co-57	300
Co-60	600
Cd-109	300
Ba-133	300
Cs-137	120

3.4 HPGe Geometric variation

A 1 μCi Cs-137 source dated February 2012 was used to determine the response of the HPGe detector to sources at various ranges. The source was placed in a holder above the detector face. A 150 s spectrum was recorded on contact and at heights of (2.6 ± 0.3) cm, (6.2 ± 0.3) cm, (9.4 ± 0.3) cm, (11.5 ± 0.3) cm, and (14.7 ± 0.3) cm.

3.5 CZT Evaluation

An effort was made to objectively compare the HPGe detector to another type of detector, namely a Cadmium Zinc Telluride (CZT) detector. This data collection was performed by the course instructors, so precise settings for the electronics chain were not available at the time of this report. The information that was available for this experiment is recorded in table 2.

4 Results

4.1 MCA performance

4.2 HPGe Resolution and efficiency

The spectra from the assorted sources were analyzed using Python and the PeakUtils library [4] in order to determine a relationship between channel number and energy. The detected peaks were correlated to known gamma emission spectra for these sources and a linear fit was performed on this data. A plot of the data and the linear fit can be seen in figure 3. Based on the $R^2 > 0.9999$ value, it was determined that further analysis could be conducted in terms of energy vice channel number, and the spectra were converted accordingly.

The spectrum for the Na-22 source showed significant photopeaks, as expected (see figure 4). The principle gamma emission from the Na-22 source is visible at E=(1274.0 ± 0.1) keV, (see equation 1). The largest peak in this spectrum corresponded to the annhilation of the positrons from the source, corresponding to an energy of 511 keV. These gamma rays produced secondary scattering events via the process of Compton Scattering. This process produced a continuous spectrum (due to the three-body nature of the products of Compton Scattering event), the maximum energy (see equation 2) produces an observable drop in the energy which corresponds to the maximum energy of the scattered electrom from these events. This is visible as a "Compton Edge" [2]. This feature appears to one degree or another in most of the spectra recorded for this report.

$$E_\gamma = m_e \times c^2 = 511 \, \text{keV} \tag{1}$$

$$E_s^{Max} = E_\gamma \left(1 - \frac{1}{1 + \frac{2E_\gamma}{m_e c^2}}\right) \tag{2}$$

The spectrum for the Mn-54 source (see figure 5) showed a single peak at 835 keV and no other visible features. This corresponds to its electron capture decay, which occurs with a branching frequency of greater than 0.9999 [5].
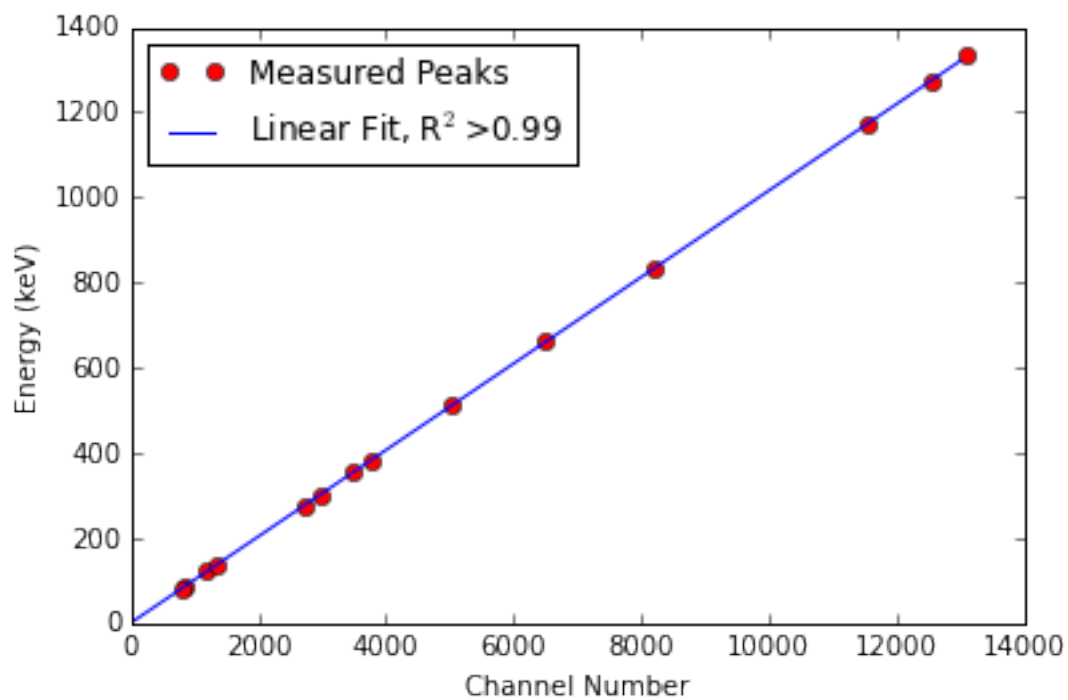
6

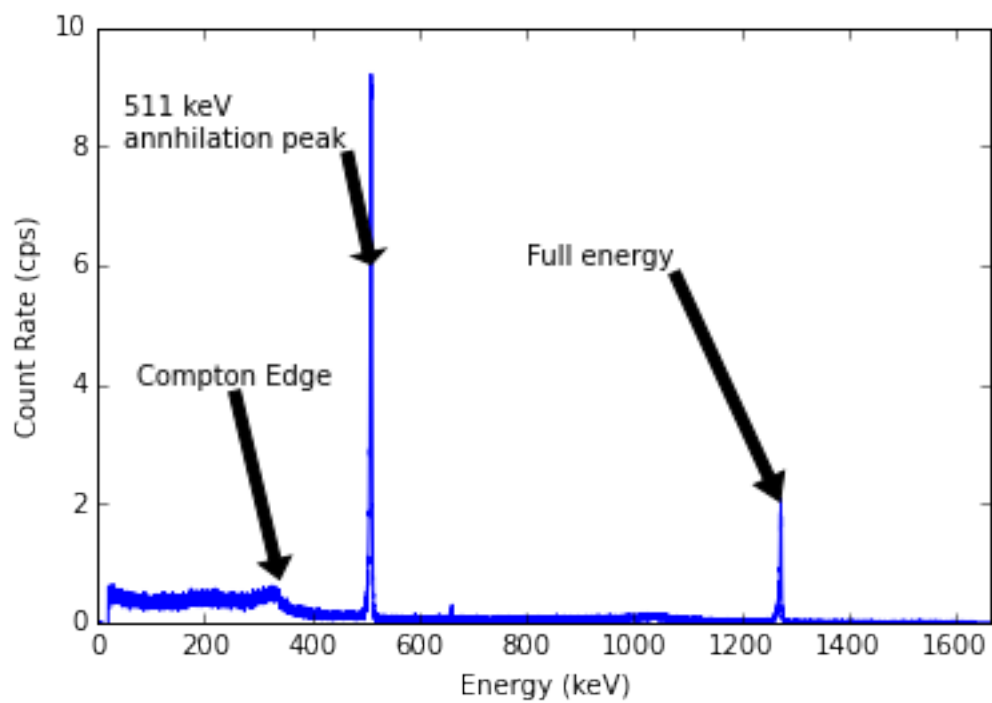Figure 3: HPGe Energy/Channel Relationship

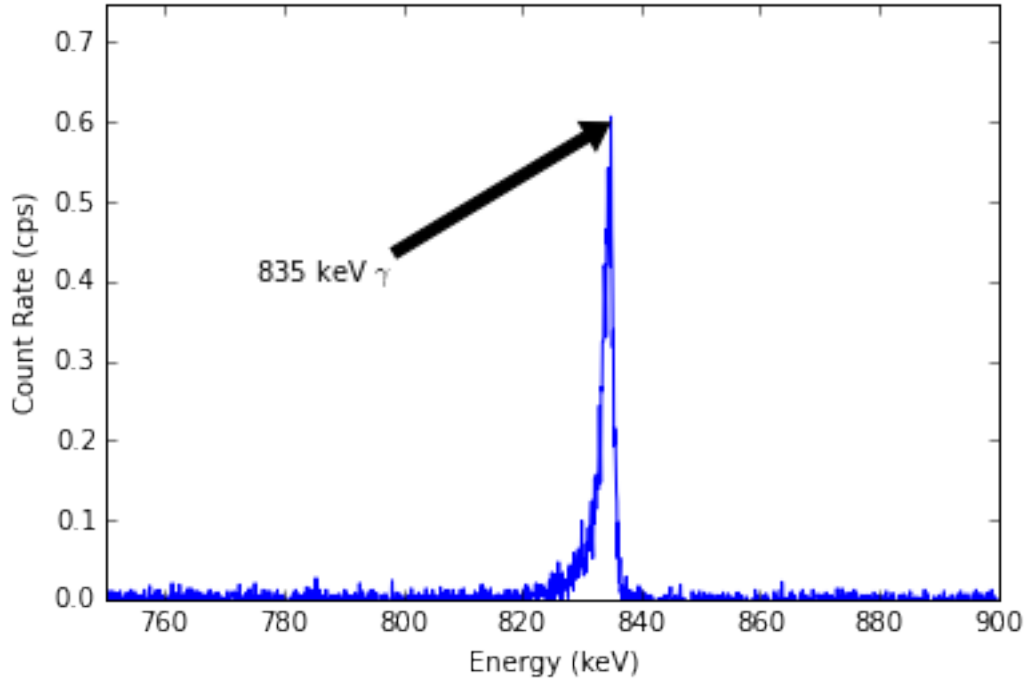Figure 4: Na-22 emission spectrum for HPGe detector

Figure 5: Mn-54 emission spectrum for HPGe detector

Two isotopes of Cobalt were examined, Co-57 and Co-60. Co-57 decays via several modes, only three of which have significant branching fractions (>1%). The lowest energy of these, an electron capture at 14.4 keV was low enough energy that it was not visible in the background-corrected spectrum (due to the prevalence of X-rays in the low-energy region below approximately 20 keV). The remaining two peaks are closely spaced at 122 keV and 136 keV, making them a good mechanism to evaluate the resolution of a detector. As expected, the two peaks were distinct on the plotted spectrum, as can be seen in figure 6. The distinct peaks also provide the opportunity to qualitatively verify the branching ratios. The magnitudes of a gaussian fit to the 122 keV and 136 keV were 15.7 cps and 1.9 cps respectively. The ratio of these values, 8.3 ± 0.5, is within error of their given branching ratios, 85.6 / 10.7 = 8.01 [5].

The spectrum for Co-60 (figure 7) shows the expected peaks at 1174 keV and 1332 keV. These peaks should show up with equal branching ratios but instead display a ratio of 1.20 ± 0.14. Further
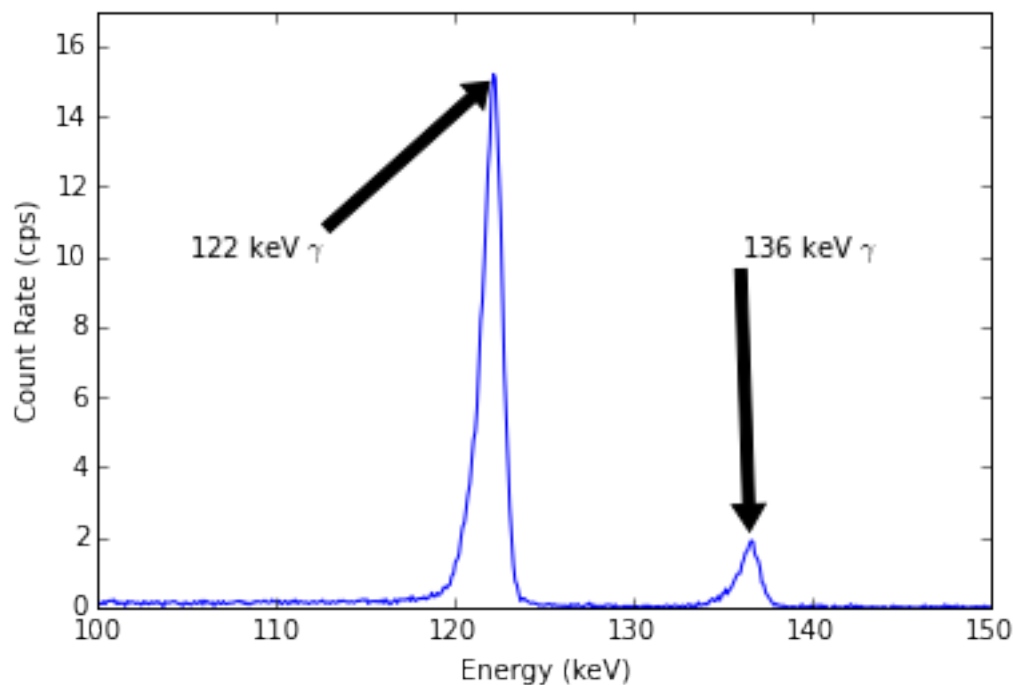
8

Figure 6: Co-57 emission spectrum for HPGe detector

analysis is appropriate to determine if this reflects a difference in the efficiency of these peaks as this experiment showed the detector photoefficiencies at these energies to be 0.0043 and 0.0036 respectively (see table 3).

Cadmium 109 (figure 8) produced the expected peak at 88.04 keV and little else of note.

Barium 133 (figure 9) had five discernable peaks at 81 keV, 276 keV, 303 keV, 356 keV and 384 keV.

Cs-137 exhibited a strong peak at 662 keV. In addition, the plot in figure 10 showed not just a compton edge at 477 keV but also the full range of the compton continuum, higlighted in the figure.
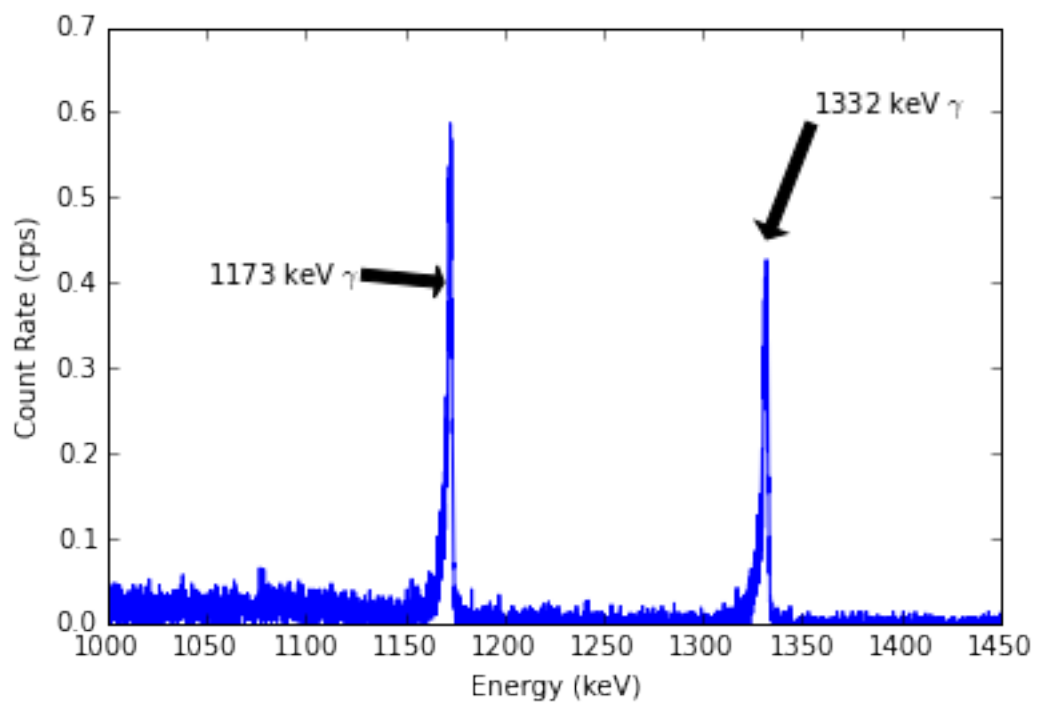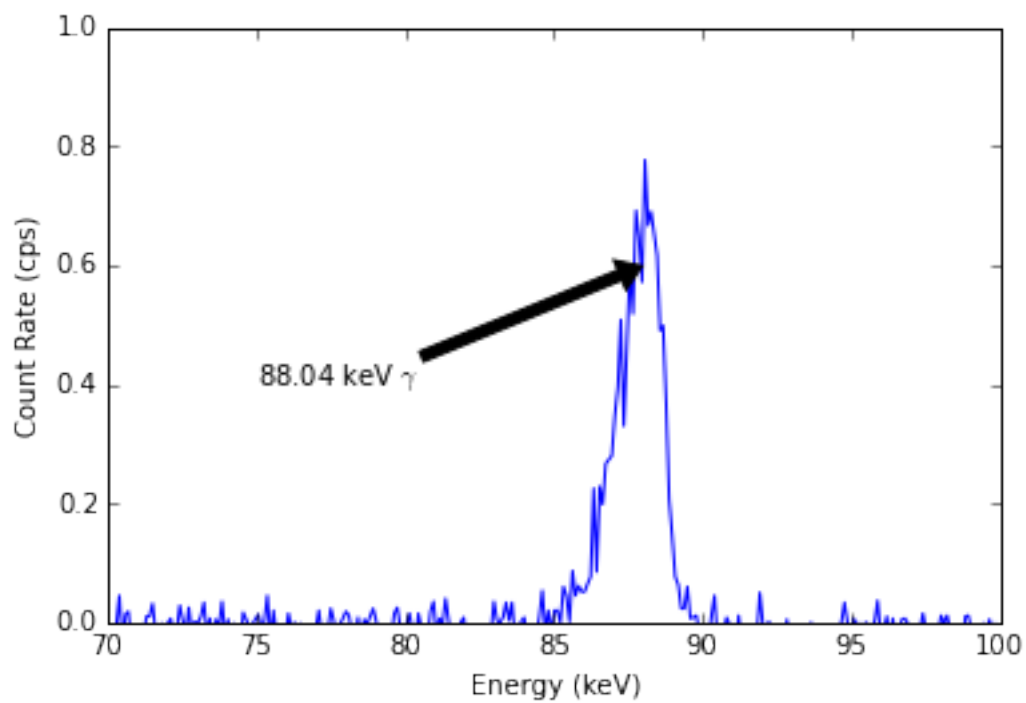
Figure 7: Co-60 emission spectrum for HPGe detector
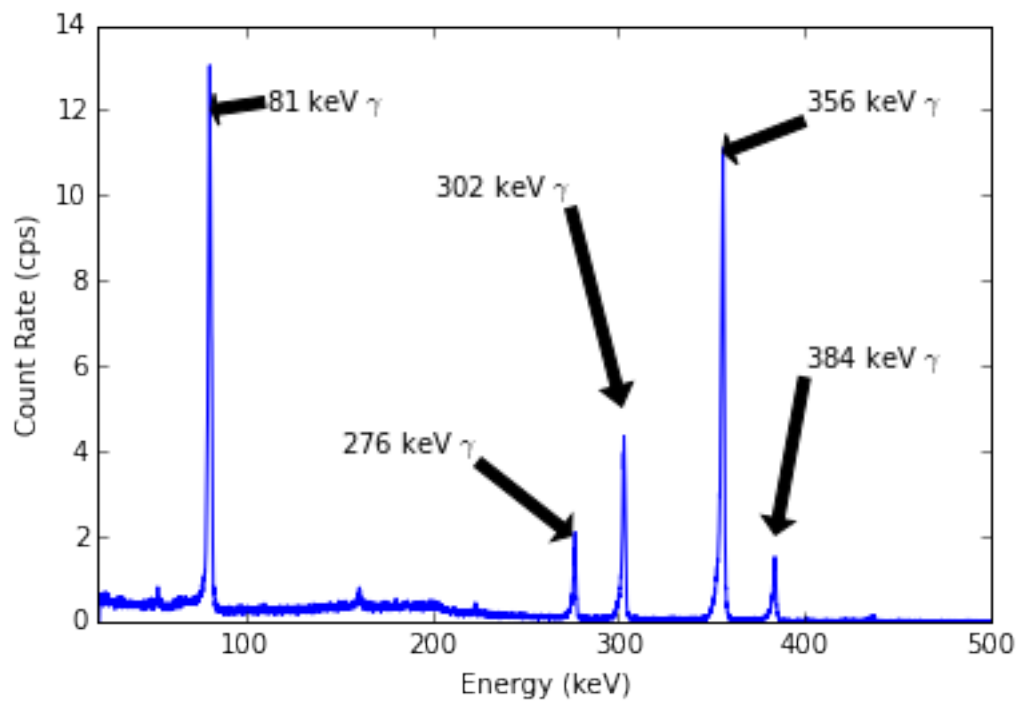

Figure 8: Cd-109 spectral for HPGe detector
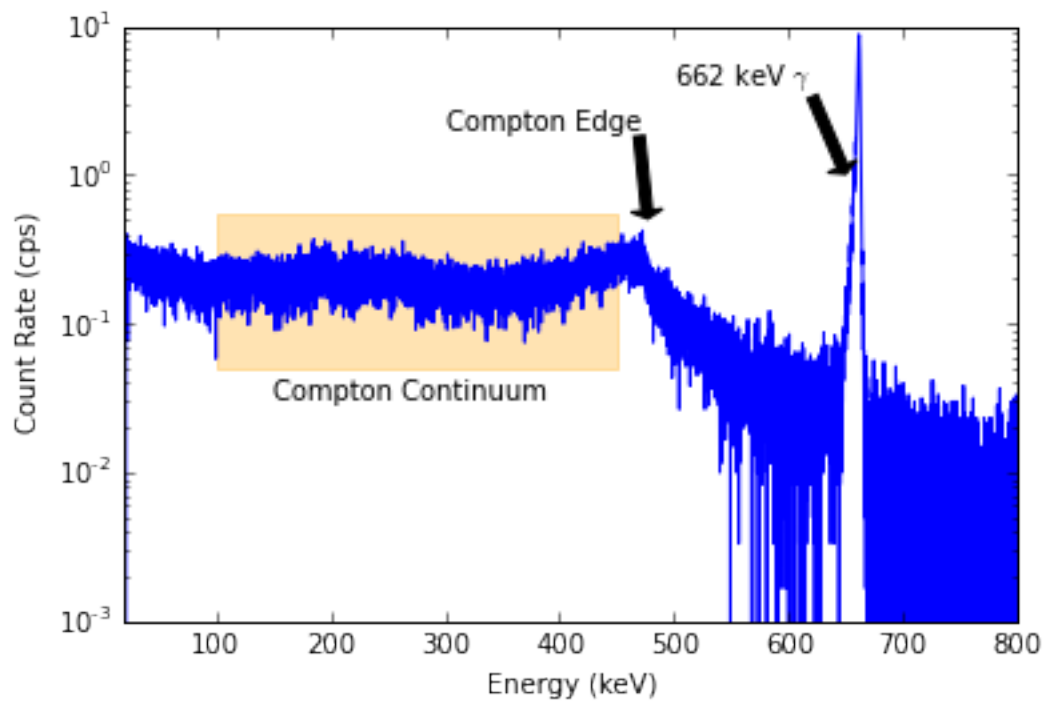
Figure 9: Ba-133 spectral for HPGe detector

Figure 10: Cs-137 spectral for HPGe detector

Table 3: Efficiency of HPGe Detector

Source	Energy ($\pm$ 0.1 keV)	FWHM (keV)	Photopeak (cps $\times$ keV)	Total (cps $\times$ keV)	Photopeak efficiency
Na-22	511	2.83	25.4	2339	0.011
	1274	2.75	4.48	2339	0.0019
Mn-54	835	1.73	0.861	82.5	0.010
Co-57	122	1.05	15.7	413.2	0.038
	136	1.06	1.90	413.2	0.0046
Co-60	1173	2.25	1.07	250.4	0.0043
	1332	2.32	0.893	250.4	0.0036
Cd-109	88.04	1.22	0.882	42.65	0.021
Ba-133	81	1.51	19.47	1509	0.013
	276	1.36	2.520	1509	0.0017
	303	1.36	5.613	1509	0.0037
	356	1.41	15.03	1509	0.010
	384	1.53	2.109	1509	0.0014
Cs-137	662	1.82	15.33	1334	0.011

In order to determine the detector efficiency for each of the photopeaks from the sources, the spectral data representing each of the peaks were segregated out and treated separately for this portion. For each prominent spectral feature, an attempt was made to determine the resolution of the detector chain for that energy. In order to conduct this analysis, a gaussian curve of arbitrary amplitude was fit to the data near the peak. The fitted amplitude represented the photopeak amplitude; the fitted σ was used with equation 3 [2] to determine the FWHM of the peak (corresponding to the resolution of the detector). The results of this analysis are recorded in table 3.

$$FHWM = 2\sigma\sqrt{2\ln 2} \qquad (3)$$

In order to examine the geometric response of the HPGe detector, spectra were taken for a Cs-
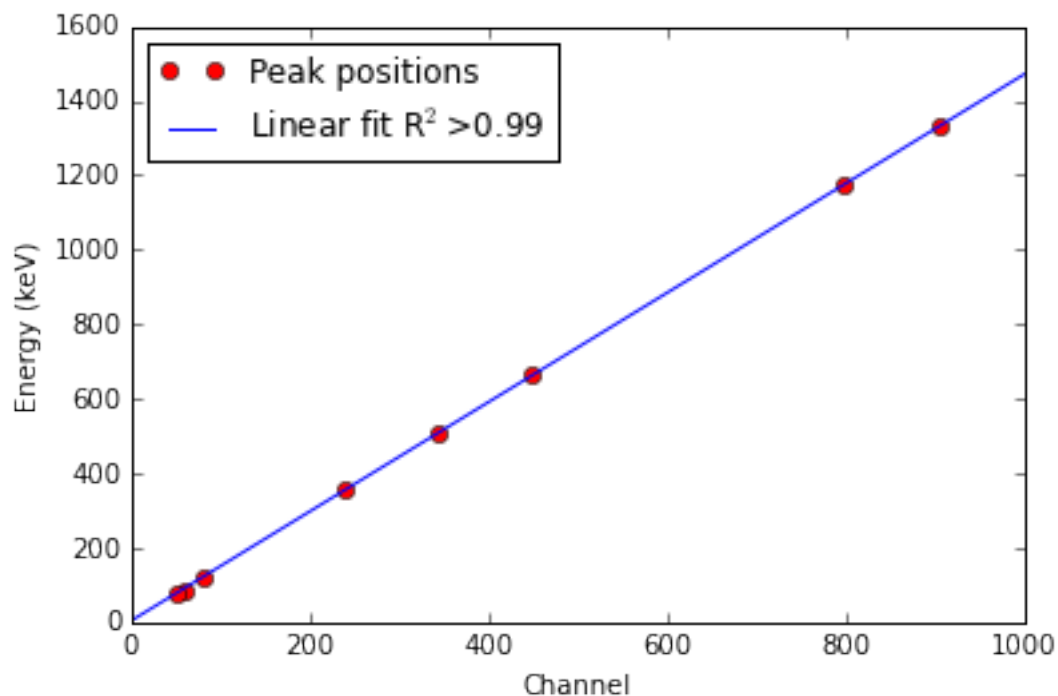
Figure 11: CZT Energy/Channel relationship

137 source at a variety of distances. These spectra are shown in figure **??**. These spectra show that the height of the peak as compared to the height of other features (notably the compton edge and continuum) shrinks at short distances, indicating high deadtime. In fact, the on-contact deadtime was 87%, as compared to a deadtime of 1.7% for a height of 14.7 cm.

4.3 CZT Performance

A similar analysis to that described for the HPGe detector above was applied to the spectra recorded by class staff for a Cadmium Zinc Telluride detector. These can be seen in figures 12, 13, 14, 15, 16, and 17. Prominent features are identified in the figures and the results of resolution and efficiency calculations are provided in table 4. It was immediately apparent that the CZT detector had significantly lower resolution than the HPGe detector, with many spectral features either weakly present or invisible. As a result, the calculations had to be made with far fewer peaks. The peaks that were available, however, made for a still-excellent energy to channel number relationship, as seen in figure 11.
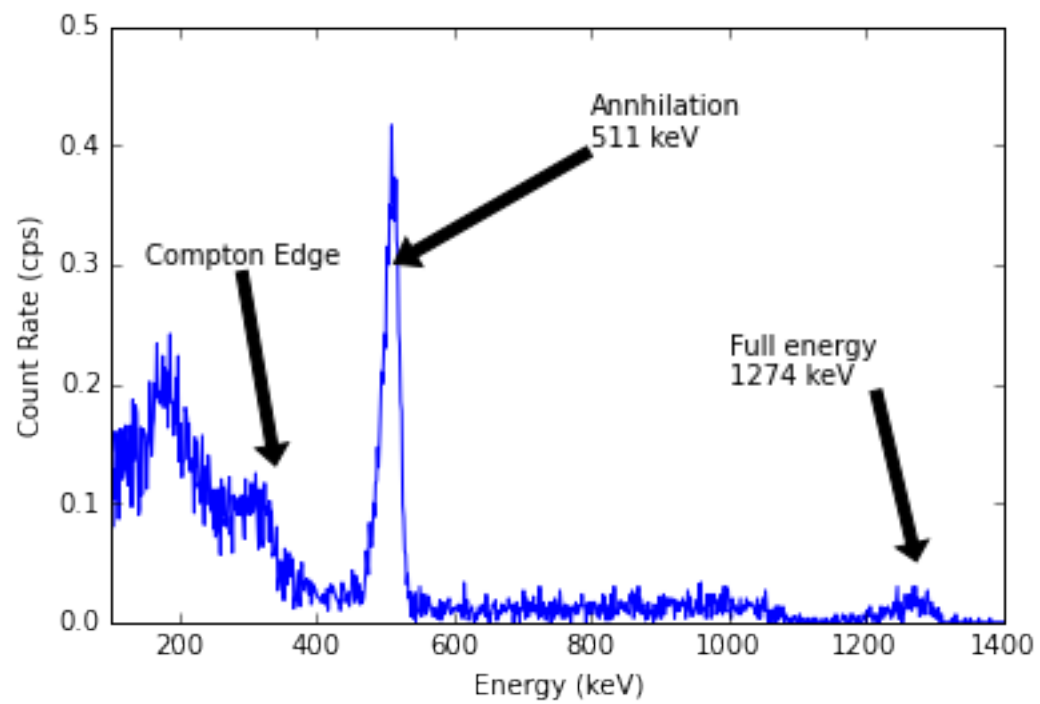
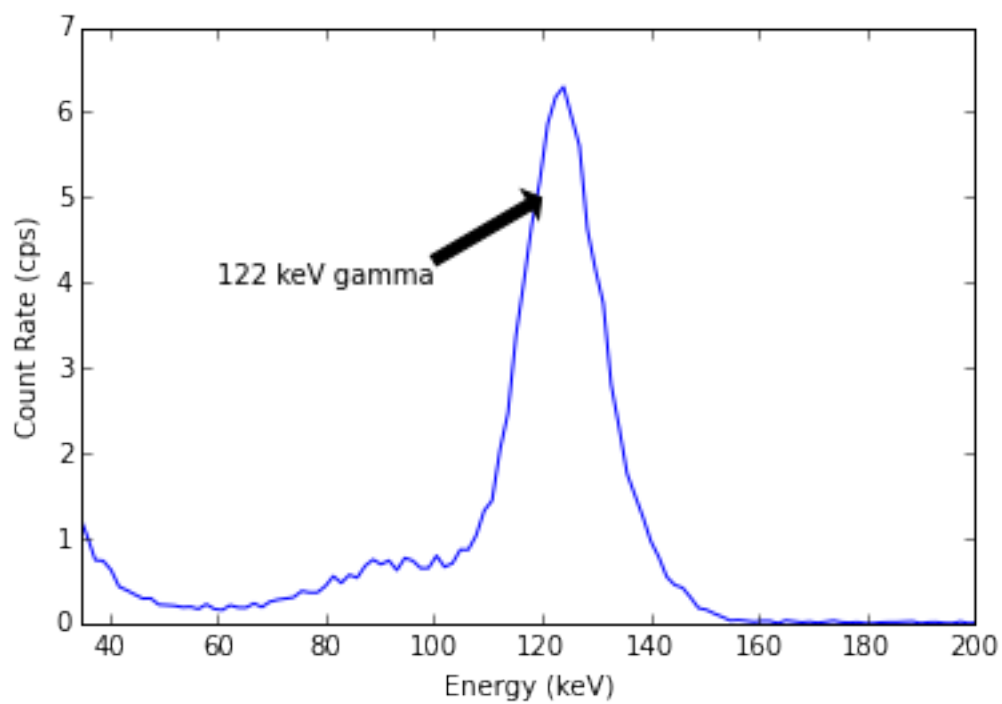Figure 12: Na-22 spectrum for CZT detector
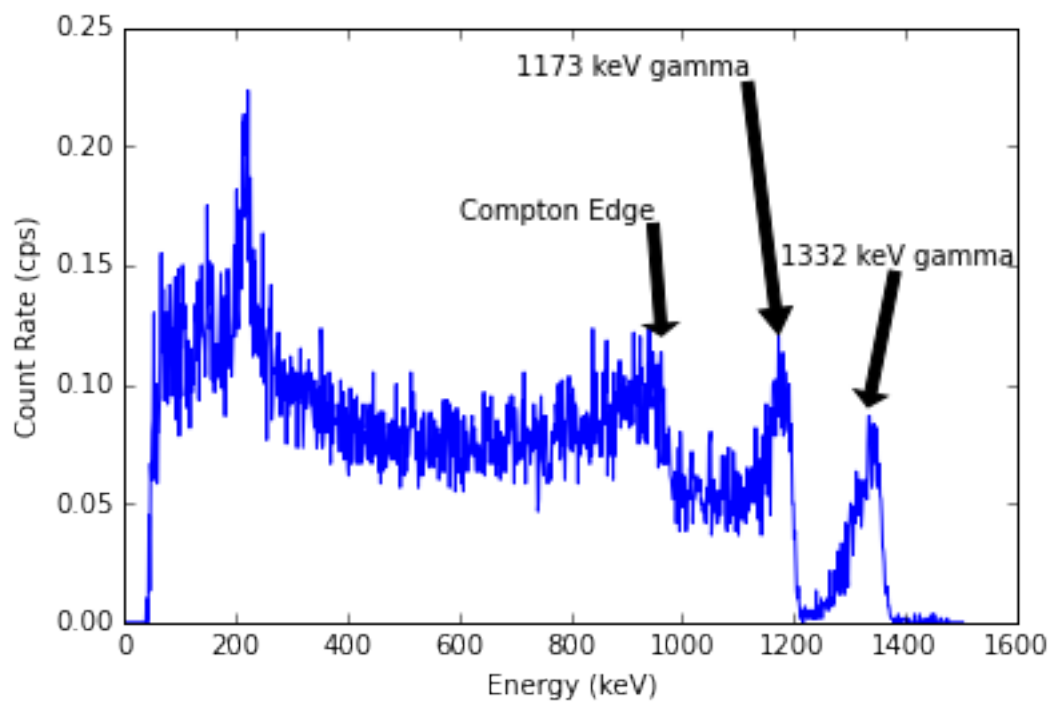
Figure 13: Co-57 spectrum for CZT detector

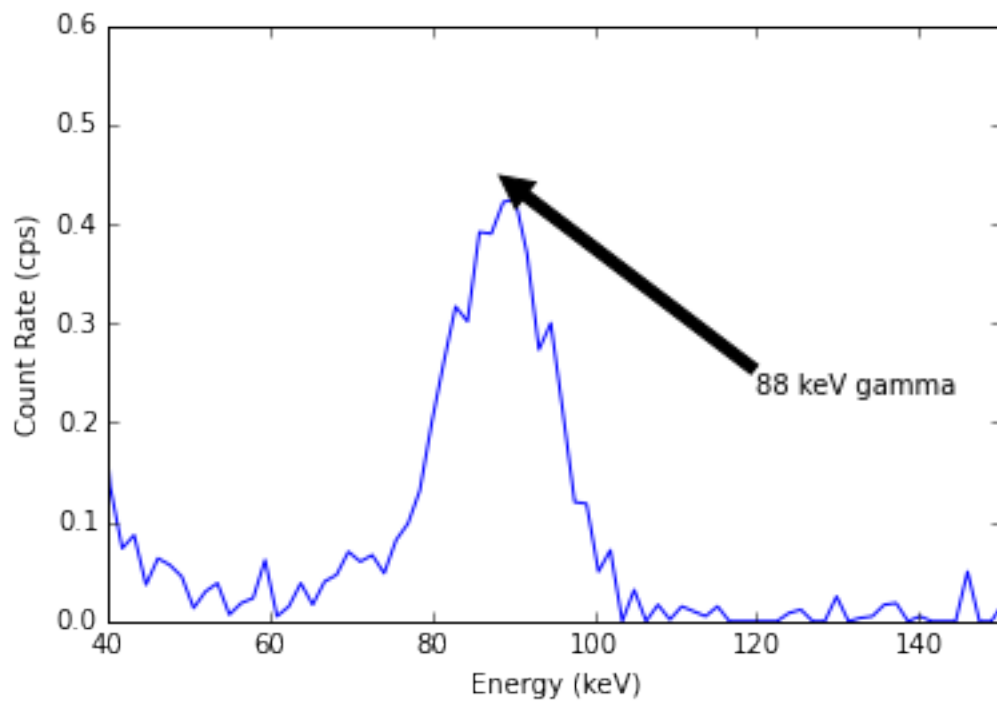Figure 14: Co-60 spectrum for CZT detector
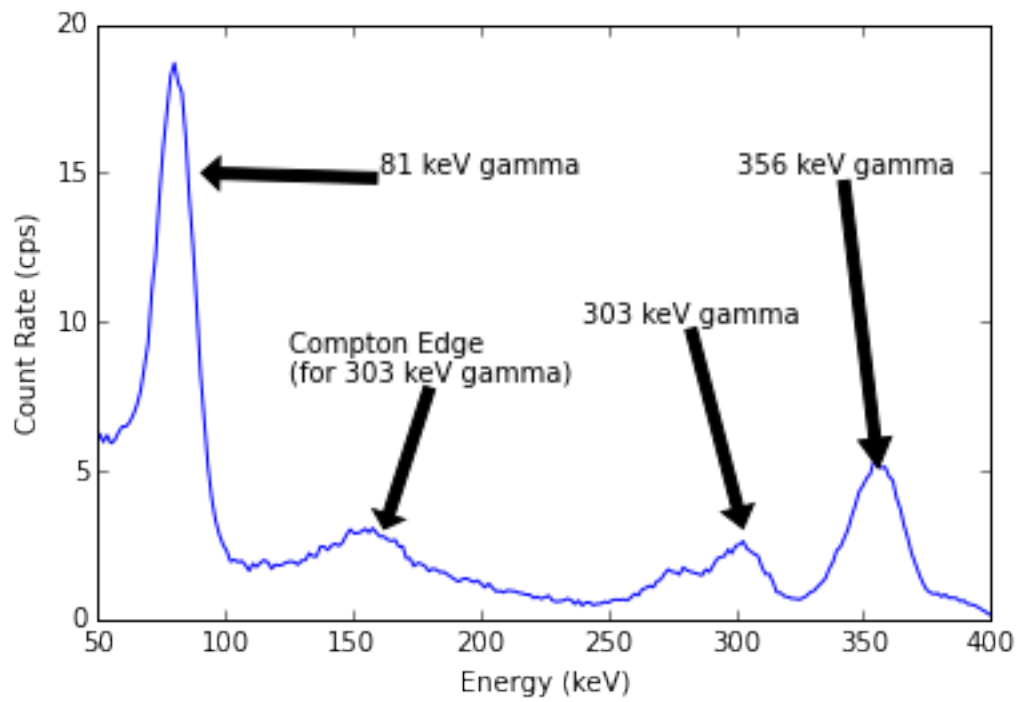
Figure 15: Cd-109 spectrum for CZT detector

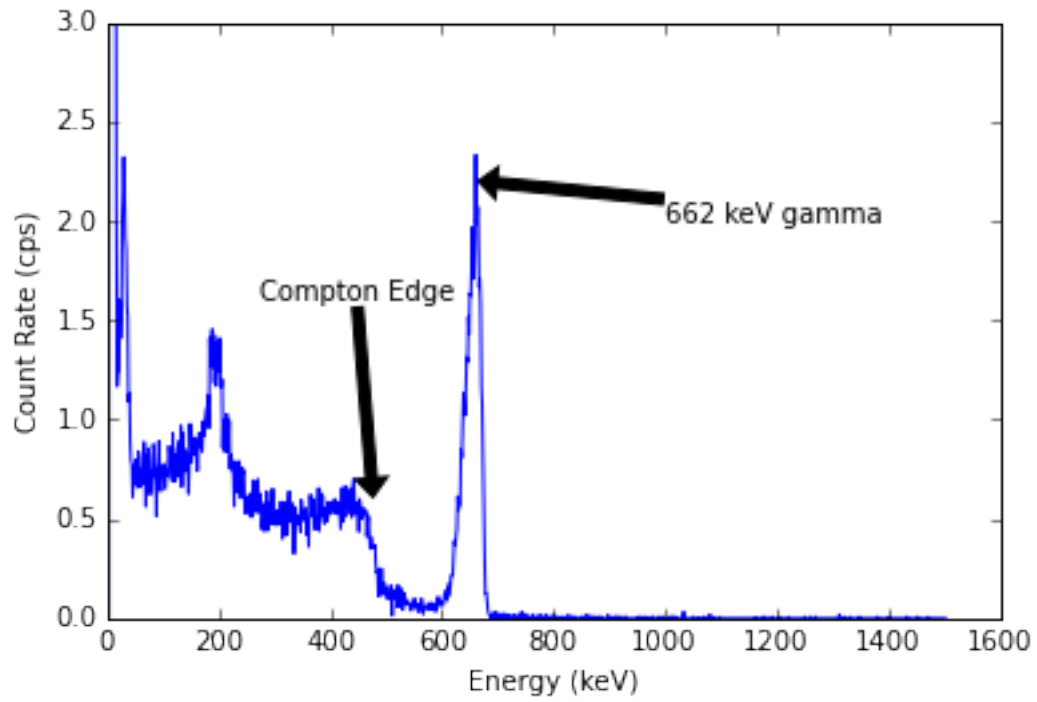Figure 16: Ba-133 spectrum for CZT detector

Figure 17: Cs-137 spectrum for CZT detector

Table 4: Efficiency of CZT Detector

Source	Energy ($\pm$ 0.1 keV)	FWHM (keV)	Photopeak (cps $\times$ keV)	Total (cps $\times$ keV)	Photopeak efficiency
Na-22	511	21.7	8.17	50.8	0.16
	1274	50.0	0.89	50.8	0.018
Co-57	122	13.5	85	111	0.77
Co-60	1173	60.1	5.7	71.51	0.080
	1332	43.2	3.13		0.044
Cd-109	88.04	11.4	4.94	13.10	0.38
Ba-133	80.99	20.7	349	880	0.40
	356	19.7	106	880	0.12
Cs-137	662	23.6	49.3	4314	0.011

5 Conclusion

The ORTEC 927 ASPEC MCA was determined to perform within the ranges required for spectral analysis, with sufficient resolution and linear response at a variety of input voltages. The performance of an HPGe detector was analyzed for a variety of well-characterized sources. Its resolution was found to be excellent, with full-width, half-max (FWHM) typically in the range of 1-3 (see table 3). A CZT detector was also analyzed which displayed FWHM values 10-20x larger than the HPGe detector, but with photoefficiencies that were higher than the HPGe by approximately the same magnitude. This fit with the findings of Perez-Andujar, et al [6]. Some statistical analysis was applied for error propogation purposes, but it would be instructive to collect more data in the future in more controlled scenarios in order to more directly compare these two detectors. Specifically, the collection times for the CZT detector were significantly longer, and the reasons for this were not clear as this data was provided to the author rather than collected directly.

References

[1] A Giaz, L Pellegri, S Riboldi, et al. "Characterization of large volume 3.5 ″× 8 ″LaBr 3: Ce detectors". In: *Nuclear Instruments and Methods in Physics Research Section A: Accelerators, Spectrometers, Detectors and Associated Equipment* 729 (2013), pp. 910–921.

[2] Nicholas Tsoulfanidis. *Measurement and detection of radiation*. CRC press, 2013. ISBN: 1439894655.

[3] P. Fougeres, P. Siffert, M. Hageali, et al. "CdTe and Cd1−xZnxTe for nuclear detectors: facts and fictions". In: *Nuclear Instruments and Methods in Physics Research Section A: Accelerators, Spectrometers, Detectors and Associated Equipment* 428.1 (1999), pp. 38–44. ISSN: 0168-9002. DOI: `https://doi.org/10.1016/S0168-9002(98)01578-2`. URL: `http://www.sciencedirect.com/science/article/pii/S0168900298015782`.

[4] Web Page. 2017. URL: `http://pythonhosted.org/PeakUtils/index.html`.

[5] Web Page. 1998. URL: `http://nucleardata.nuclear.lu.se/toi/`.

[6] A Perez-Andujar and L Pibida. "Performance of CdTe, HPGe and NaI (Tl) detectors for radioactivity measurements". In: *Applied radiation and isotopes* 60.1 (2004), pp. 41–47. ISSN: 0969-8043.